ADVANCED HEALTHCARE MATERIALS

Supporting Information

for *Adv. Healthcare Mater.*, DOI 10.1002/adhm.202300305

Gold-Enhanced Brachytherapy by a Nanoparticle-Releasing Hydrogel and 3D-Printed Subcutaneous Radioactive Implant Approach

*Mariia Kiseleva, Théophraste Lescot, Svetlana V. Selivanova and Marc-André Fortin**

Supporting Information

Gold-enhanced Brachytherapy by a Nanoparticle-Releasing Hydrogel and 3D-Printed Subcutaneous Radioactive Implant Approach

*Mariia Kiseleva, Théophraste Lescot, Svetlana V. Selivanova, and Marc-André Fortin**

Section 1. Characterization results of the synthesized AuNPs

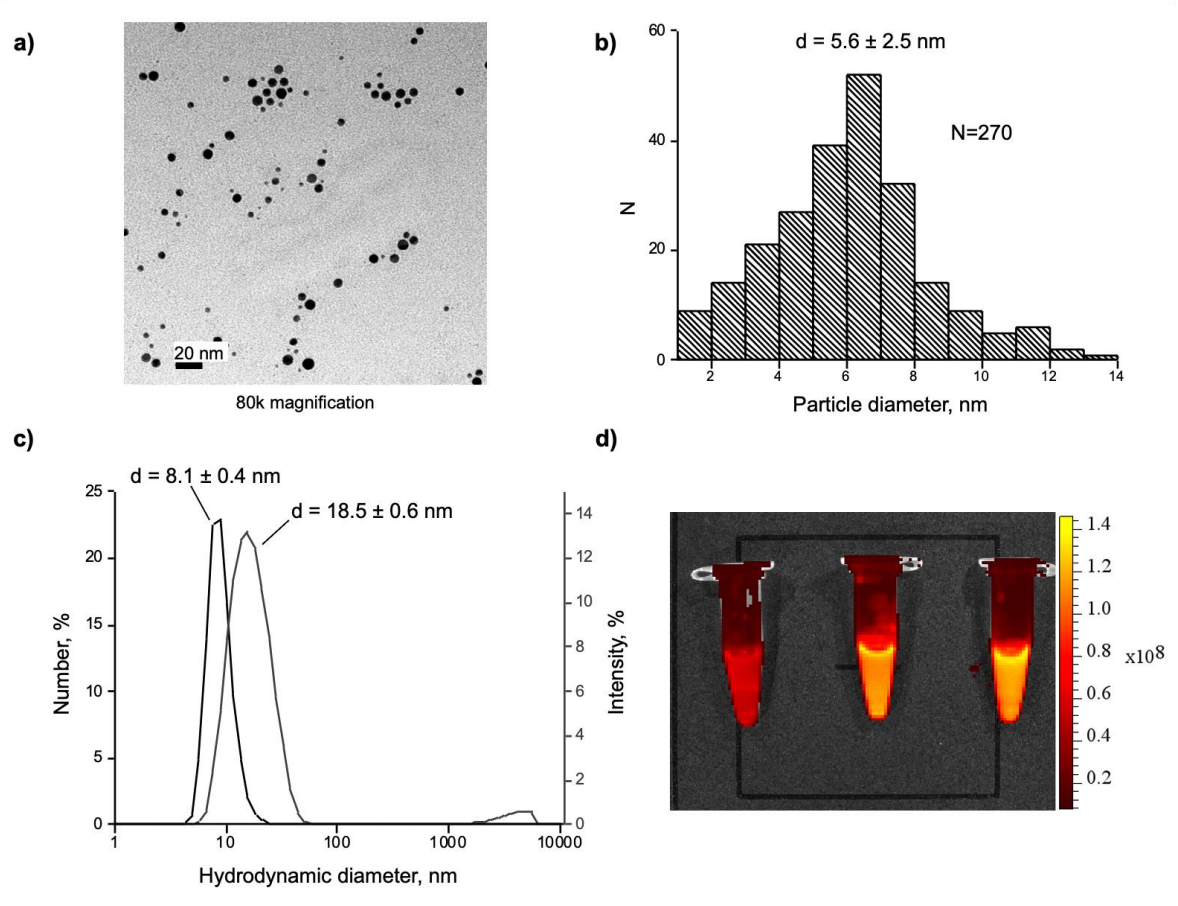

Figure S1. Characterization of AuNPs-PEG-DFO/Cy 5 (nanoparticles). a) TEM analysis with 80k magnification, scale bar is 20 nm; b) Size distribution analysis extracted from the TEM data; c) Intensity-weighted and number-weighted size distributions obtained by DLS; d) Fluorescent image of vials filled with AuNPs-PEG-DFO/Cy5 merged with a photograph obtained by the IVIS Lumina III imaging system (PerkinElmer, Waltham, MA, USA), the concentration of AuNPs-PEG-DFO/Cy5 from left to right is 0.01, 0.5, and 0.1 mg/ml. Excitation peak 640 nm, emission peak 665 nm. The scale is in values of epifluorescence counts. Materials and Methods of the experiments can be found in *Supporting Information* of Kiseleva *et al.*, *ACS Biomater. Sci. Eng.* **2022**, 8, 1200-1214.[1]

Section 2. Radiolabeling and in vitro stability of [^{89}Zr]Zr-AuNPs

Materials

[^{89}Zr]Zr-oxalate ($t_{1/2}$ = 78.41 h, C_4O_8Zr, 265 g mol^{-1}, 1350 MBq mL^{-1}) was purchased from the University of Alabama (Birmingham, USA). [^{89}Zr]Zr-chloride ($t_{1/2}$ = 78.41 h, Cl_4Zr) was purchased from the University of Sherbrooke (Sherbrooke, Canada). Radioactivity measurements were performed using a calibrated dose calibrator (Atomlab 100, Biodex Medical Systems, Shirley, USA). Oxalic acid ($C_2H_2O_4$, 90.03 g mol^{-1}, 99.999% trace metals basis), sodium carbonate (Na_2CO_3, 105.99 g mol^{-1}, anhydrous, 99.999% trace metals basis), ethylenediaminetetraacetic acid (EDTA, disodium salt, dihydrate, $C_{10}H_{16}N_2O_8$, 372.24 g mol^{-1}) were purchased from Millipore Sigma. 4-(2-hydroxyethyl)-1-piperazineethanesulfonic acid (HEPES, $C_8H_{18}N_2O_4S$, 238.3 g mol^{-1}) was obtained from Fisher BioReagents. Phosphate buffer saline (PBS, pH 7.4) was purchased from Gibco by Life Technologies (Grand Island, USA). Silica gel thin-layer chromatography plates (TLC silica gel 60 F254) were purchased from Millipore (Catalog Number 105715, Canada). All solutions were prepared with ultrapure water (OmniTrace Ultra, for trace metal analysis, Millipore) to minimize potential contamination with metal ions. Where needed, the pH of the solutions was adjusted with NaOH (5 mol L^{-1}) or HCl (5 mol L^{-1}) and verified using pH paper (Catalog Number BDH35311.604, VWR Chemicals BDH®, Canada).

Simulated vaginal fluid (SVF, one of the incubation media) was prepared as previously described.[2] Briefly, sodium chloride (NaCl, 58.44 g mol^{-1}, ≥99.0%, 3.51 g), potassium hydroxide (KOH, 56.11 g mol^{-1}, ≥85.0%, 1.4 g), calcium hydroxide ($Ca(OH)_2$, 74.09 g mol^{-1}, ≥95.0%, 0.22 g), bovine serum albumin (lyophilized powder, ≥96.0%, 0.018 g), lactic acid ($C_3H_6O_3$, 90.08 g mL^{-1}, ≥85.0%, 2.00 g), acetic acid ($C_2H_4O_2$, 60.05 g mol^{-1}, ≥99.0%, 1.00 g), glycerol ($C_3H_8O_3$, 92.09 g mol^{-1}, ≥99.0%, 0.16 g), urea (negative urine control, 0.4 g), and glucose ($C_6H_{12}O_6$, 180.16 g mol^{-1}, ≥96.0%, 5.00 g), all purchased from Millipore Sigma (Oakville, Canada), were added to 900 mL of nanopure water and stirred until complete

dissolution. The pH of the mixture was adjusted to 4.5 using 0.1 N HCl, and the final volume was adjusted to 1 L using nanopure water (a water purifier, Purelab Flex, ELGA LabWater).

Methods

[^{89}Zr]Zr-oxalate (10.81 MBq) in oxalic acid (1 mol L^{-1}, 40 µL) was neutralized with Na_2CO_3 (1 mol L^{-1}, 30.8 µL) to pH 7.0 and diluted with HEPES buffer (100 mmol L^{-1}, 100 µL). The AuNPs-PEG-DFO (0.1 mg mL^{-1}) in water (1 mL) were then added, and the reaction was allowed to proceed at ambient temperature for one hour.

Radiolabeling efficiency of AuNPs-PEG-DFO was measured by thin-layer chromatography (TLC) analysis of the crude reaction mixture using aluminum TLC plates coated with silica gel as a stationary phase and EDTA (100 mmol L^{-1}, pH 5) as a mobile phase. TLC plates were cut perpendicularly into 9 fractions, and each part was measured in a well counter. [^{89}Zr]Zr-AuNPs remained at the origin, and free ^{89}Zr migrated with the solvent front. Radiolabeling efficiency of the ^{89}Zr-chelation was determined as a ratio (%) of measured activity at the origin to total activity on the TLC plate.

The aliquots (50 µL) were taken from the vial with formed [^{89}Zr]Zr-AuNPs, put to the labeled Eppendorfs, and diluted five times with PBS 1X (200 µL, pH 7), saline (200 µL, 154 mmol L^{-1}, pH 7), SVF (200 µL, pH 4.5), mouse serum (200 µL, pH 7). The Eppendorfs were then incubated for 1, 24, 48, and 72 h. At each time point, an aliquot of 1 µL was taken for TLC analysis. The samples with PBS 1X, SVF, and mouse serum were incubated at 37 °C to simulate physiological temperature, while the saline solution was kept at room temperature. The experiment was performed in triplicate.

Results

AuNPs radiolabeling for the stability study in different media was performed using [^{89}Zr]Zr-oxalate as a starting reagent. In this case, it is supplied in oxalic acid with a concentration of 1 mol L^{-1}. Upon neutralization with sodium carbonate, sodium oxalate ($Na_2C_2O_4$) is formed, which is a quite toxic compound (oral, mouse: LD_{50} = 5094 mg kg^{-1};

intraperitoneal, mouse: LD_{50} = 155 mg kg^{-1}; subcutaneous, mouse: LD_{50} = 100 mg kg^{-1}). In contrast, when using [^{89}Zr]Zr-chloride as a starting reagent, no toxic by-products are formed. That is why, for the *in vivo* study, the radiolabeling procedure was carried out using [^{89}Zr]Zr-chloride.

Regardless of the starting reagent used, the radiolabeling efficiency of AuNPs with ^{89}Zr was found to be >99% (confirmed by radio-TLC, Figure S2, panel a). After 1 h of incubation at RT, the activity remained at the origin of the TLC plate (between 1 and 2 cm) and appeared as a sharp peak in the graph (solid line in Figure S2, panel a). In contrast, before the addition of AuNPs, "free" ^{89}Zr in either [^{89}Zr]Zr-oxalate or [^{89}Zr]Zr-chloride form migrated with the solvent front and appeared as two wide peaks on the TLC plate, between 1.5 and 3.5 cm, and between 4 and 6.5 cm (dashed line in Figure S2, panel a). Because of the high radiochemical purity of the obtained [^{89}Zr]Zr-AuNPs, they were used without additional purification.

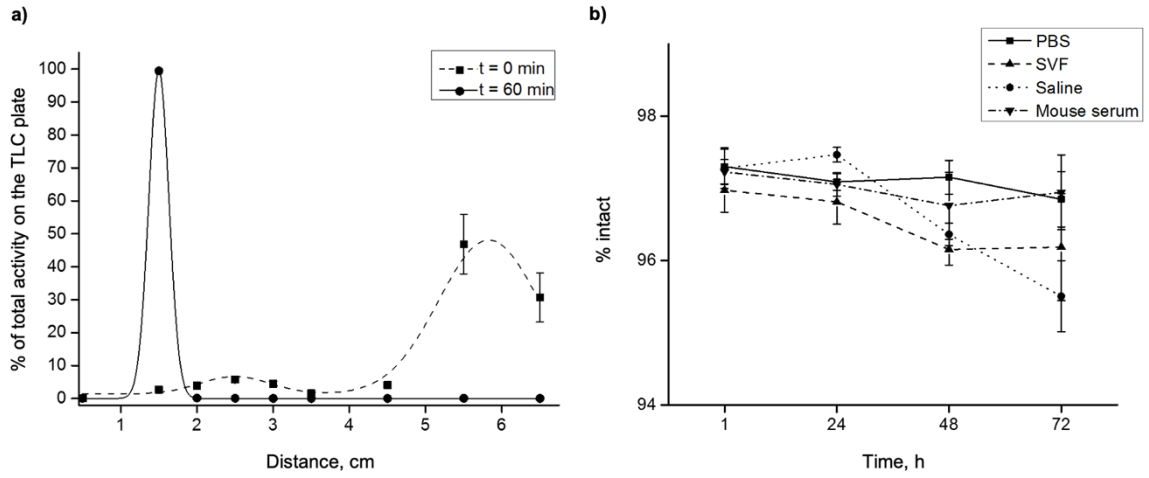

Figure S2. a) Distribution of the activity on the TLC plate before the addition of AuNPs (dashed line) and after 1 h of incubation with AuNPs at RT (solid line); b) Results of the stability study of [^{89}Zr]Zr-AuNPs in PBS, SVF, saline, and mouse serum. The data are presented as mean ± SD (n = 3).

The stability of the [^{89}Zr]Zr-AuNPs complex was challenged in different media: PBS 1X, normal saline (154 mmol L^{-1}), simulated vaginal fluid (pH 4.5), and mouse serum (Figure S2, panel b). As a result, [^{89}Zr]Zr-AuNPs remained >95% intact in all tested media after 72 h of incubation. This suggests that the radiolabeled AuNPs were highly stable in the media under

physiological conditions (isotonic solutions, 37 ºC), and no ^{89}Zr-dechelation took place. Moreover, the acidic pH 4.5 of the simulated vaginal fluid did not affect the stability of the [^{89}Zr]Zr-AuNPs.

Section 3. AuNP cytotoxicity test

Methods

HeLa cells were maintained in DMEM supplemented with fetal bovine serum (10%) and antibiotic solution (penicillin-streptomycin, 1%). CRL 2616 cells were maintained in keratinocyte-serum-free media with human recombinant EGF (0.1 ng mL^{-1}), bovine pituitary extract (0.05 mg mL^{-1}), antibiotic solution (penicillin-streptomycin, 1%), and additional calcium chloride (44.1 mg L^{-1}, final concentration 0.4 mmol L^{-1}). BT-474 cells were maintained in RPMI medium supplemented with fetal bovine serum (10%), antibiotic solution (penicillin-streptomycin, 1%), and insulin (0.1%). All cell lines were maintained at 37 °C in a saturated humid atmospheric chamber containing 95% air and 5% CO2. Once confluent, the cells were detached from the flask with trypsin-EDTA (0.05%), centrifuged, counted, and then resuspended in a growth medium for further experiments. Each condition of the cell culture experiments was repeated six times.

Assessment of cytocompatibility of AuNPs. AuNPs solutions at final concentrations of 6.25, 12.5, 25, 50, and 100 μg mL^{-1} were tested. AuNPs stock solution (1000 μg mL^{-1}) was sterilized using a 0.2 μm filter, and a serial dilution was performed to obtain other concentrations.

The tested cells were trypsinized, centrifuged, and resuspended at the density of 1×10^6 cells mL^{-1} in the culture medium. The cell suspension was added into each well (1×10^5 cells/well in case of CRL-2616 cells, 2×10^5 cells/well in case of HeLa cells, and 5×10^5 cells/well in case of BT-474 cells) and incubated in a 5% CO2 incubator at 37 °C for 24 h. At the end of the incubation period, AuNPs solutions of each concentration (100 μL) were layered over the

cells, the complete medium (900 µL) was added, and the plates were incubated at 37 °C for 24 h and 48 h. Control well plates containing untreated cells in complete growth media and in media with 2% DMSO were used as a negative and a positive control, respectively (for BT-474 cells, only negative control was used). Cell viability was assessed by the trypan blue dye exclusion method. For this, the cell culture medium was removed from the samples, which were then washed with PBS, followed by trypsinization. The cells were then resuspended in culture media, and an aliquot (10 µL) of the cell suspension was taken and mixed with trypan blue dye (10 µL). Cell viability was measured with a Cellometer Auto T4 cell counter (Nexcelom).

Results

Human cervical cancer (HeLa), human normal vaginal mucosa (CRL 2616), and human breast cancer (BT-474) cell lines were chosen to evaluate the cytotoxicity of the synthesized AuNPs. BT-474 cell line was selected for the tests parallel to HeLa and CRL 2616 cells to broaden the application spectrum of the formulation because the therapy of locally advanced breast cancer could also benefit from radiation treatment with AuNPs as adjuvants.[3, 4] The cytocompatibility of the AuNPs in a concentration range from 6.25 µg mL^{-1} to 100 µg mL^{-1} was evaluated using a trypan blue dye exclusion method.

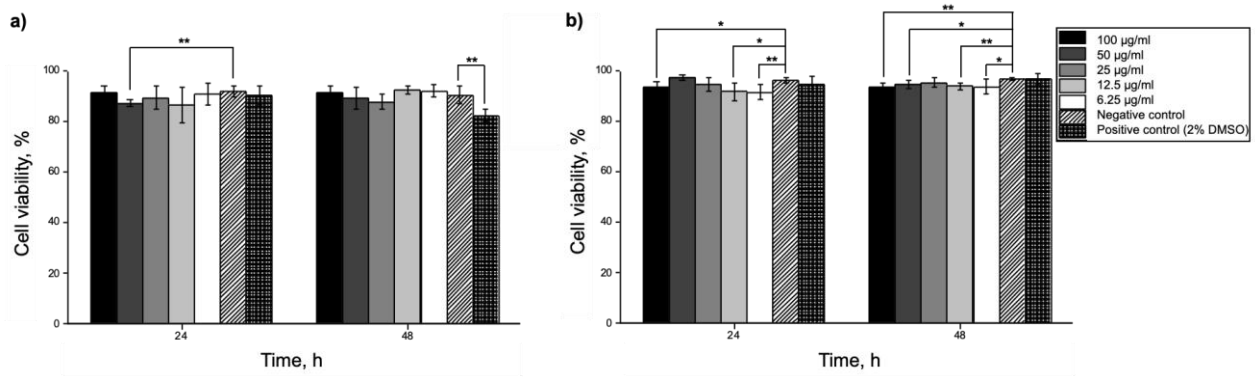

Figure S3. *In vitro* cytocompatibility of AuNPs of different concentrations with a) HeLa cells, b) CRL-2616 cells. The data were analyzed using the one-way ANOVA test followed by the Post Hoc Tukey HSD test and are presented as mean ± SD (n = 6), $p < 0.05$ (*), $p < 0.005$ (**).

The cell viabilities of the HeLa and CRL-2616 cells are shown in Figure S2, whereas the results of the experiment with BT-474 cells can be found in Figure S5. It was observed that after two days of direct contact with the tested formulations, HeLa and CRL-2616 cells remained over 87% and 93% viable, respectively. This result indicates that the synthesized AuNPs demonstrated no obvious cytotoxicity and exhibited good cytocompatibility in the tested concentration range. Based on this outcome, 100 μg mL^{-1} concentration was selected for further *in vivo* experiments. Moreover, we found that the AuNPs formulations did not affect the proliferation of the HeLa and CRL-2616 cells (see Figure S4).

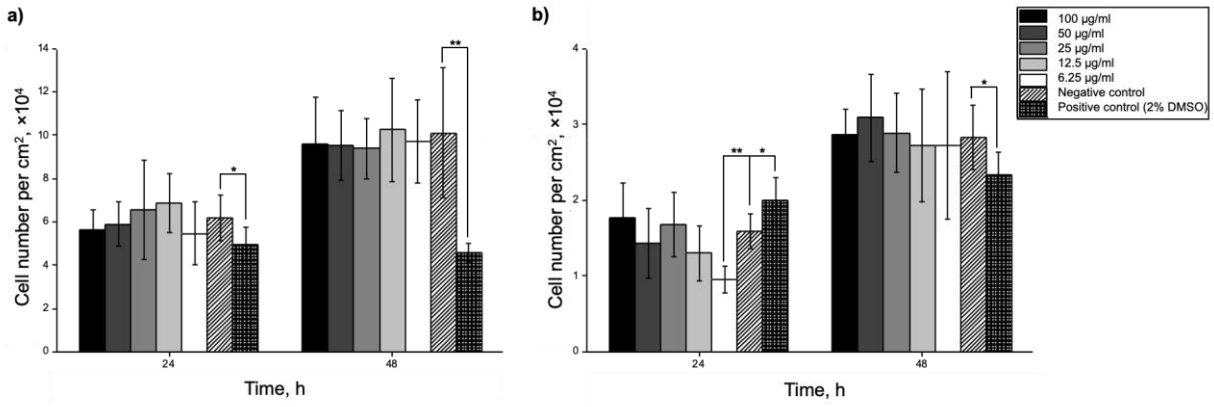

Figure S4. HeLa (a) and CRL-2616 (b) cell number per cm^2 after incubation with AuNPs of different concentrations, seeding density for the HeLa cells was 2.1 x 10^4 cells cm^{-2} and 1.1 x 10^4 cells cm^{-2} for the CRL-2616 cells. The data were analyzed using the one-way ANOVA test followed by the Post Hoc Tukey HSD test and are presented as mean ± SD (n = 6), $p < 0.05$ (*), $p < 0.005$ (**).

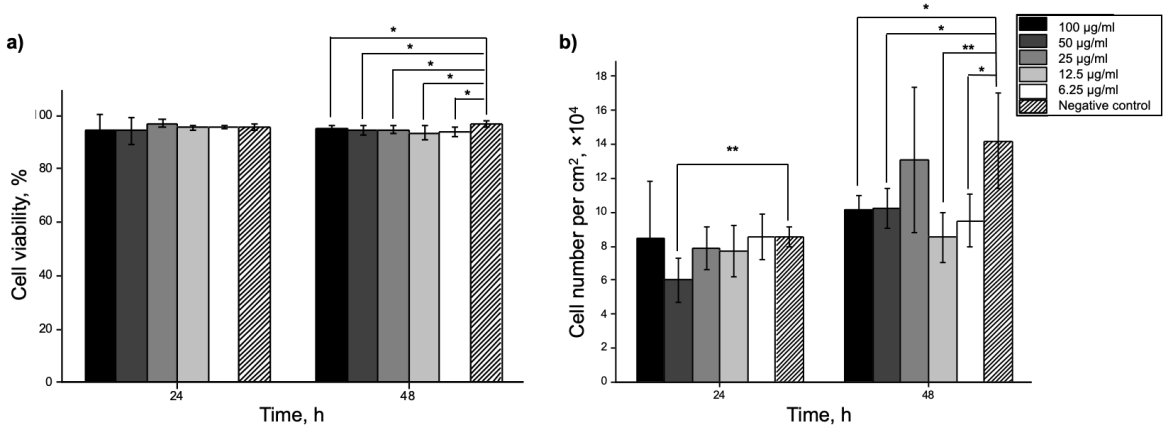

Figure S5. BT-474 viability (a) and cell number per cm2 (b) after incubation with AuNPs of different concentrations, the seeding density was 5.3 x 10^4 cells cm^{-2}. The data were analyzed using the one-way ANOVA test followed by the Post Hoc Tukey HSD test and are presented as mean ± SD (n = 6), $p < 0.05$ (*), $p < 0.005$ (**).

Section 4. Biocompatibility of the PF-A hydrogel with and without AuNPs

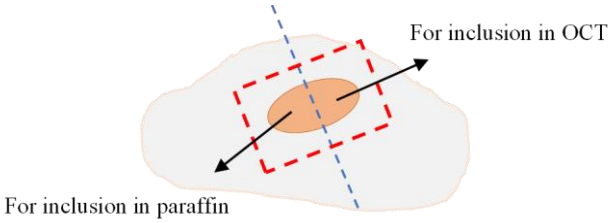

Figure S6. Representative schematic of tissue sampling for inclusion in paraffin (H&E staining) and inclusion in OCT (immunofluorescence staining).

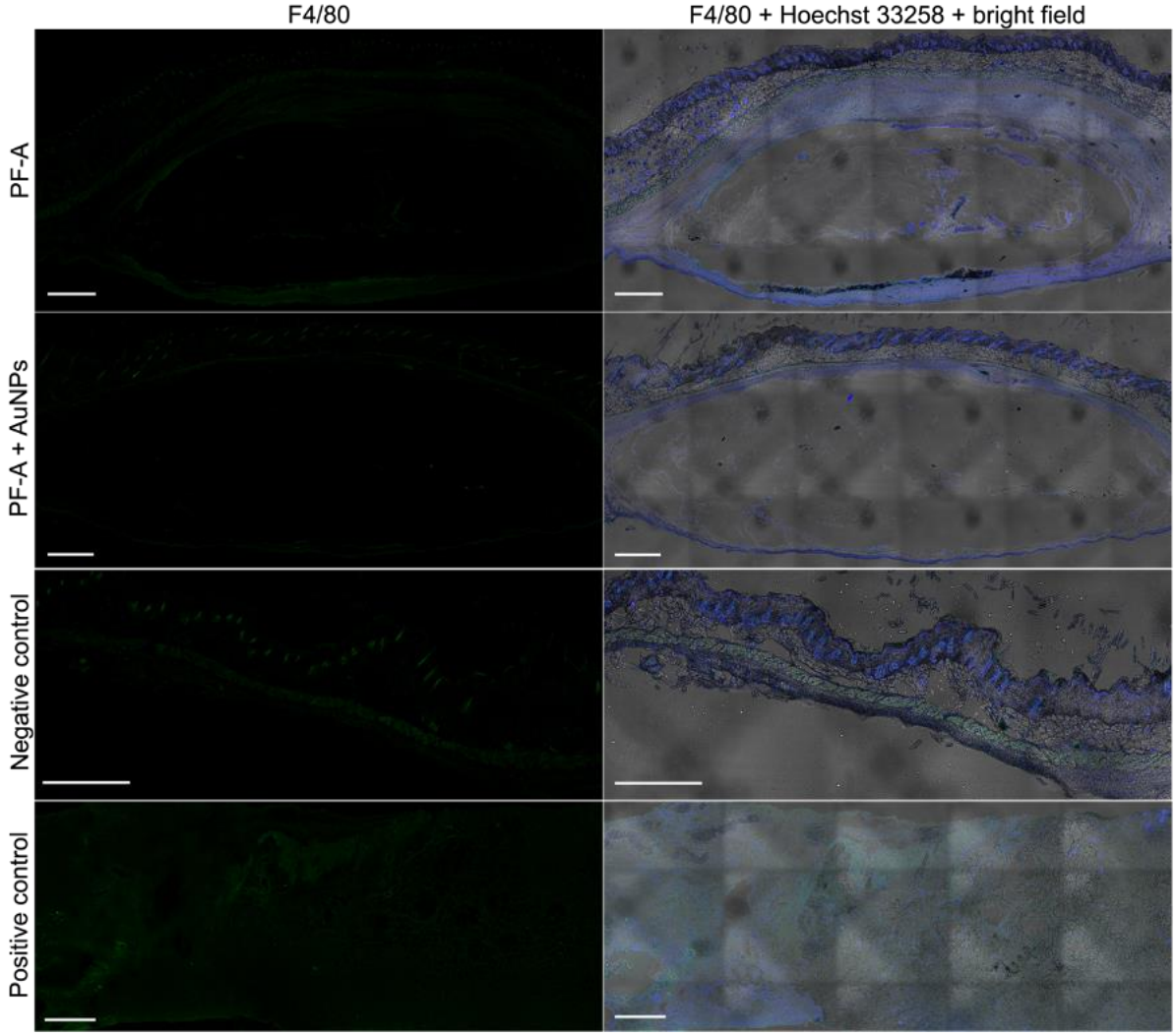

Figure S7. Results of nuclear and F4/80 macrophages immunostaining of the PF-A and PF-A + AuNPs hydrogels with surrounding tissue at day 14 post administration (isotypic control).

The skin of infected mice was used as a positive control, whereas the skin from the opposite flank of the experimental mice was used as a negative control. Cell nuclei are stained in blue; macrophages are stained in green. The thickness of the slide is 20 μm. Scale bar 500 μm.

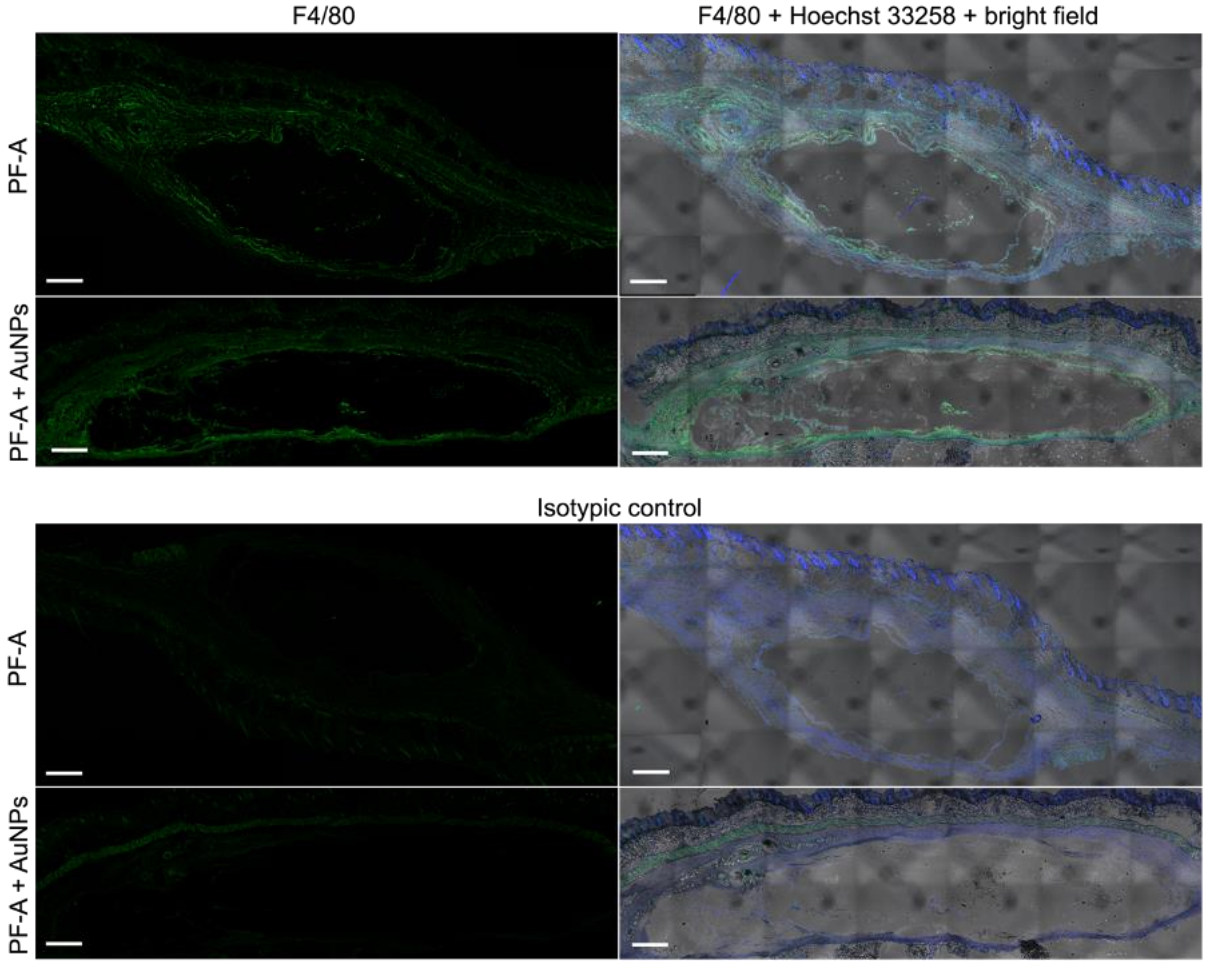

Figure S8. Outliers in the results of nuclear and F4/80 macrophages immunostaining with isotypic controls of the *PF-A* and *PF-A + AuNPs* hydrogels with surrounding tissue at day 14 post-administration. The skin of infected mice was used as a positive control, whereas the skin from the opposite flank of the experimental mice was used as a negative control. Cell nuclei are stained in blue; macrophages are stained in green. The thickness of the slide is 20 μm. Scale bar 500 μm.

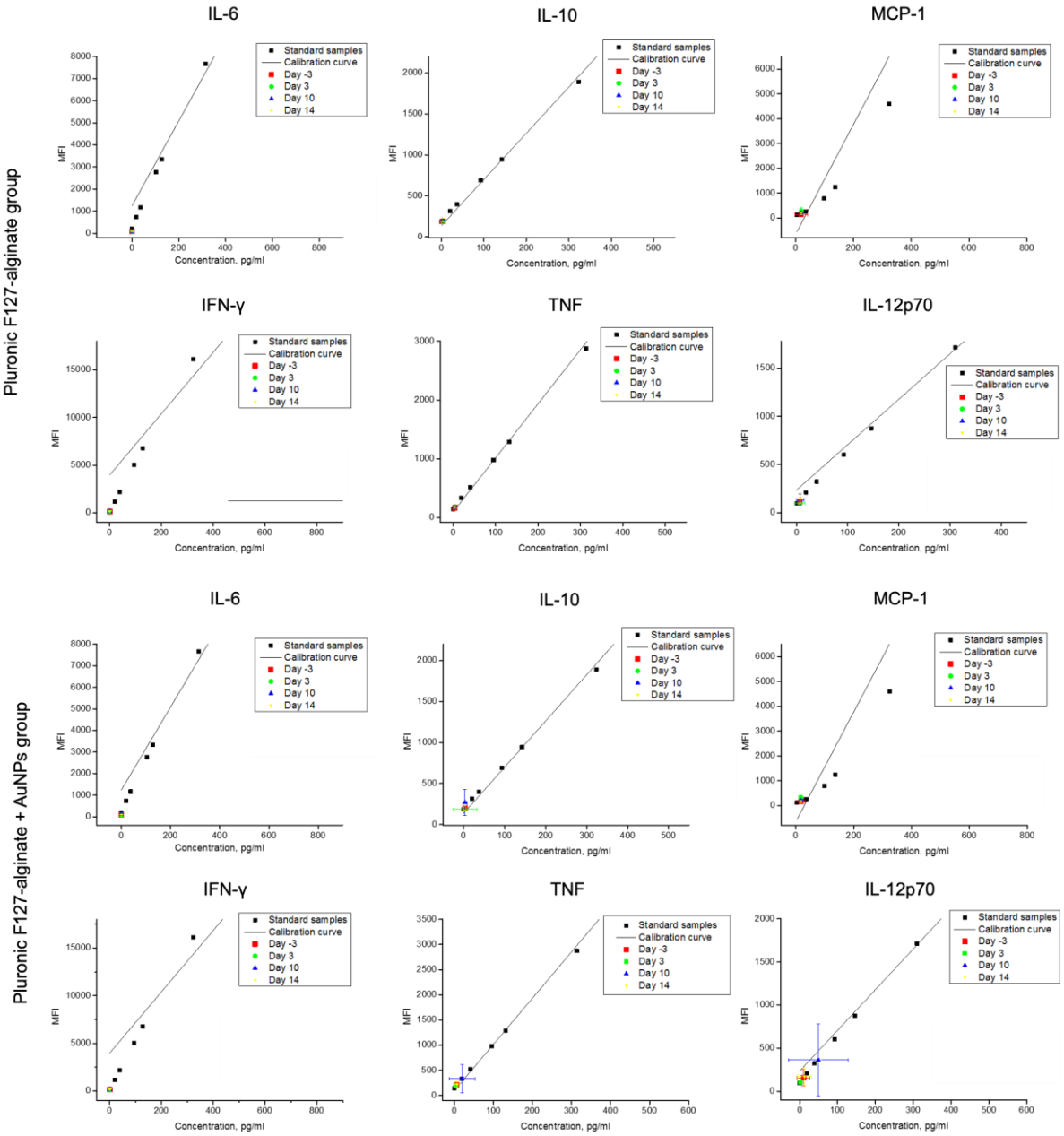

Figure S9. Expression of the cytokines at days -3, 3, 10, and 14 for the *PF-A* group and *PF-A + AuNPs* group. The data are presented as mean ± SD (n = 6) for each time point.

Section 5. In vivo release of ^{89}Zr[Zr]-AuNPs

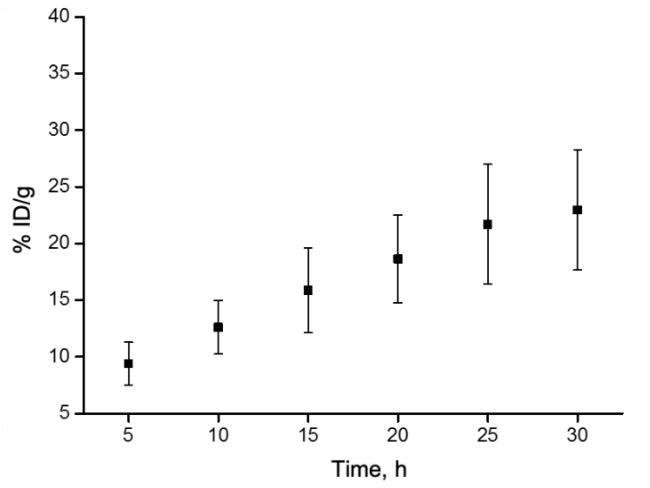

Figure S10. Accumulation of the [^{89}Zr]Zr-AuNPs in the bladder in the first 30 min p.i. The data are presented as mean ± SD (n = 3).

Section 6. Body weight of mice and histological assessment of tumors (AuNP-releasing hydrogels applied as a 3D-printed subcutaneous implant: radiosensitizing effect on tumors)

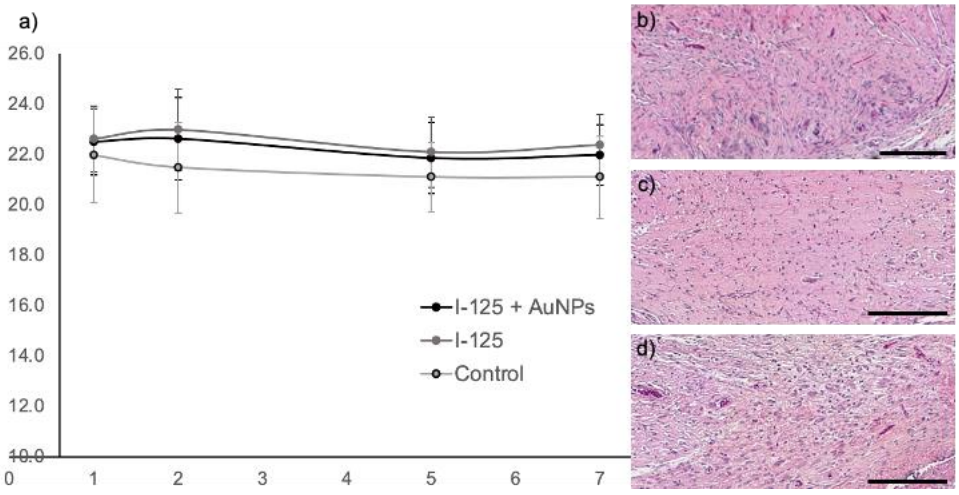

Figure S11. a) Body weight of mice during 7-day study, with day 1 being the surgery day. Data are presented as mean ± standard deviation (n = 5). Histological assessment of the tumors, representative samples from the: b) I-125 + AuNPs group, c) I-125 group, and d) control group. Scale bar is 200 μm.

Section 7. Measurement of PF127 and alginate content in the hydrogel by TGA analysis

Materials

Thermal analysis of the lyophilized hydrogel sample (preparation is described in *Section 5.2.2* of the *Experimental* section) with a mass of 1 mg was performed on a TGA 851 (Mettler-Toledo) apparatus. The sample was heated from ambient temperature up to 800 °C at a heating rate 5 °C/min in the air at a flow rate of 20 ml min^{-1}. The results of this analysis are presented as a thermogravimetric (TG) curve (a weight loss of the sample as a function of temperature) and the first derivative of the TG curve (derivative thermogravimetric curve, DTG).

Results

Figure S10 shows the thermal behavior of the lyophilized PF127-alginate sample in the air atmosphere. The TG and corresponding DTG curves suggest that, under heating, the material underwent four degradation steps.

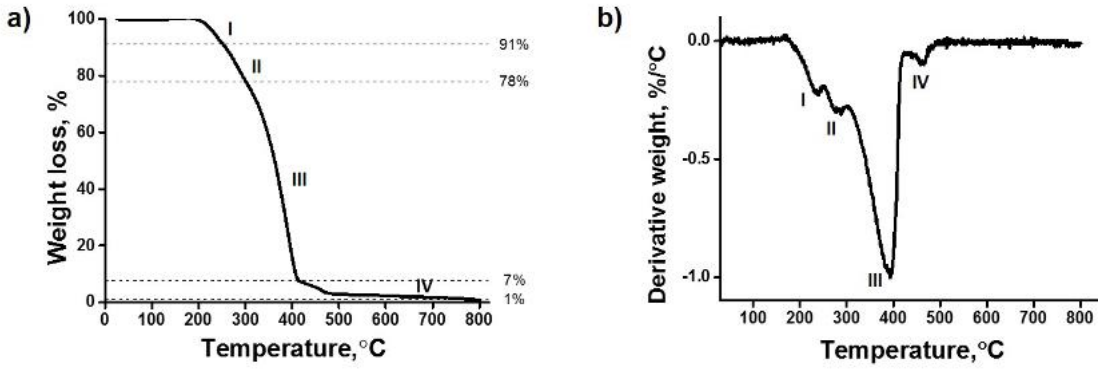

Figure S12. Thermal behavior of PF127-alginate sample. a) The thermogravimetric (TG) curve; b) the derivative thermogravimetric (DTG) curve. The degradation steps are identified as I, II, III and IV.

The sample demonstrated initially a dehydration process (I) followed by degradation of the polymer network in two overlapping steps (II and III), and, finally, the formation of $NaCO_3$

and $CaCO_3$ and their decomposition into Na_2O and CaO (IV) at higher temperatures.[5] The parameters of each degradation step can be found in Table S1.

Table S1. Degradation steps parameters.

Step №	Process	Temperature interval, ºC	T_{max}*, ºC	Weight loss, %
I	Dehydration	200-250	235	9
II	Degradation of alginate	250-300	285	22
III	Degradation of PF127	300-425	393	93
IV	Formation of $NaCO_3$ and $CaCO_3$	425-800	462	99

*T_{max} is the temperature of the maximum weight loss rate

At about 200 ºC, the material started to exhibit the first weight loss corresponding to the evaporation of the residual water molecules that, most probably, were tightly bound to alginate that has hydrophilic carboxyl and hydroxyl groups in the structure. The second step observed within the temperature range of 250-300 °C after the removal of moisture could be related to the thermal degradation of alginate chains. The weight loss is typically associated with the destruction of glycosidic bonds and the decarboxylation reaction of polysaccharide chains.[6, 7] Moreover, this degradation process corresponds to the beginning of the thermal decomposition of PF127. The third stage, observed between 300 °C and 425 °C, should correspond to the complete degradation of PF127 component. It is reported that PF127 polymer exhibits one sharp degradation step with T_{max} (the temperature of the maximum mass loss rate) at around 400 ºC.[8, 9] During this step, the sample lost the major part of its weight since PF127 is the main component of the polymer system. DTG thermogram showed T_{max} of this step at 393 ºC, which is close to the data found in the literature.[8, 9] The last degradation step between 425-800 °C can be associated with the formation of $NaCO_3$ and $CaCO_3$ salts in the crucible with their following decomposition into Na_2O and CaO.[5] Overall, around 99% of the sample had disintegrated at the end of the experiment leaving behind 1% of its weight in the form of carbonized residue and Na_2O and CaO salts.

References:

[1] M. Kiseleva, M.M. Omar, E. Boisselier, S.V. Selivanova, M.A. Fortin, A Three-Dimensional Printable Hydrogel Formulation for the Local Delivery of Therapeutic Nanoparticles to Cervical Cancer, *ACS Biomater. Sci. Eng.* **2022**, *8*, 1200-1214.
[2] G.M. Soliman, G. Fetih, A.M. Abbas, Thermosensitive bioadhesive gels for the vaginal delivery of sildenafil citrate: in vitro characterization and clinical evaluation in women using clomiphene citrate for induction of ovulation, *Drug Development and Industrial Pharmacy* **2017**, *43*, 399-408.
[3] J. Xing, J. Zeng, J. Yang, T. Kong, T. Xu, W. Roa, X. Wang, J. Chen, Ieee, *Gold-based nanoparticles for breast cancer diagnosis and treatment*, in: 2007 Ieee International Symposium on Circuits and Systems, Vols 1-11, Ieee, New York, 2007, pp. 2882-+.
[4] S. Yook, Z.L. Cai, Y.J. Lu, M.A. Winnik, J.P. Pignol, R.M. Reilly, Intratumorally Injected Lu-177-Labeled Gold Nanoparticles: Gold Nanoseed Brachytherapy with Application for Neoadjuvant Treatment of Locally Advanced Breast Cancer, *Journal of Nuclear Medicine* **2016**, *57*, 936-942.
[5] W. Zhao, Y. Qi, Y. Wang, Y. Xue, P. Xu, Z. Li, Q. Li, Morphology and Thermal Properties of Calcium Alginate/Reduced Graphene Oxide Composites, *Polymers (Basel)* **2018**, *10*.
[6] S. Jana, M. Kumar Trivedi, R.M. Tallapragada, Characterization of Physicochemical and Thermal Properties of Chitosan and Sodium Alginate after Biofield Treatment, *Pharmaceutica Analytica Acta* **2015**, *6*.
[7] N. Patel, D. Lalwani, S. Gollmer, E. Injeti, Y. Sari, J. Nesamony, Development and evaluation of a calcium alginate based oral ceftriaxone sodium formulation, *Prog Biomater* **2016**, *5*, 117-133.
[8] Q. Dou, A. Abdul Karim, X.J. Loh, Modification of Thermal and Mechanical Properties of PEG-PPG-PEG Copolymer (F127) with MA-POSS, *Polymers (Basel)* **2016**, *8*.
[9] D.T. Nguyen, V.T. Dinh, L.H. Dang, D.N. Nguyen, B.L. Giang, C.T. Nguyen, T.B.T. Nguyen, L.V. Thu, N.Q. Tran, Dual Interactions of Amphiphilic Gelatin Copolymer and Nanocurcumin Improving the Delivery Efficiency of the Nanogels, *Polymers (Basel)* **2019**, *11*.